Finger Joint Angle Estimation Based on Motoneuron Discharge Activities

Chenyun Dai, and Xiaogang Hu

***Abstract*— Estimation of joint kinematics plays an important role in intuitive human-machine interactions. However, continuous and reliable estimation of small (e.g., the finger) joint angles is still a challenge. The objective of this study was to continuously estimate finger joint angles using populational motoneuron firing activities. Multi-channel surface electromyogram (sEMG) signals were obtained from the extensor digitorum communis muscles, while the subjects performed individual finger oscillatory extension movements at two different speeds. The individual finger movement was first classified based on the EMG signals. The discharge timings of individual motor units were extracted through high-density EMG decomposition, and were then pooled as a composite discharge train. The firing frequency of the populational motor unit firing events was used to represent the descending neural drive to the motor unit pool. A second-order polynomial regression was then performed to predict the measured metacarpophalangeal extension angle using the derived neural drive based on the neuronal firings. Our results showed that individual finger extension movement can be classified with > 96% accuracy based on multi-channel EMG. The extension angles of individual fingers can be predicted continuously by the derived neural drive with R^2 values > 0.8. The performance of the neural-drive-based approach was superior to the conventional EMG-amplitude-based approach, especially during fast movements. These findings indicated that the neural-drive-based interface was a promising approach to reliably predict individual finger kinematics.**

***Index Terms*— Biosignal processing, Joint angle prediction, Motor unit, Finger movement, Motor unit decomposition.**

I. Introduction

Human-machine interactions have shown great promise in restoring motor function for individuals with neuromuscular disorders [1]–[3]. To drive these rehabilitative/assistive devices, biological signals, ranging from electrophysiological signals of the nerve system to limb biomechanical signals, are typically extracted to interface with the machine. In the past few years, we have seen substantial development in robust human-machine interface, in order to establish a reliable communication between humans and machines [4]–[6]. Specifically, the decoded neural information for the desired motor output can come from multiple sources, such as the brain, peripheral nerves, or muscles [7]–[9]. For example, motor intent has been decoded from neuronal activities of the motor cortex, and has been used to control neuroprosthesis of a subject with tetraplegia [9]. A proportional and simultaneous control of multiple degrees of freedom prostheses is also possible with decoded motor intent based on intramuscular electromyogram (EMG) signals [10].

Surface EMG (sEMG) signals have also been widely used as a control input of robot-assisted devices [11]–[13]. Global EMG features (e.g. amplitude [14] or spatial activation pattern [15]) can be used to control rehabilitation/assistive devices. However, the stability and accuracy is not satisfactory, largely due to issues of the intrinsic stability of the global EMG features and the distortion of the neural signals after a series of transformations from the brain to the muscles. Specifically, EMG signals represent a spatial and temporal superimposition of motor unit action potential (MUAP) trains from hundreds of recruited motor units (MUs). Phase and amplitude cancellation of MUAPs during superposition can distort the actual descending neural information [16]. Variations of the MUAP amplitudes or shapes affected by the volume conductive process from the muscle to the skin surface can also bias global EMG features. Lastly, external factors during the acquisition of EMG signals can also contaminate the recordings. These include a shift of the electrode location relative to the targeted muscles, motion artifact interference [17], or a variation of the baseline noise in the EMG signals.

To address these issues, a neural interface signal based on the discharge frequency of the motoneuron pool has been developed [18]. This neural interface first obtains motoneuron discharge information through decomposition of the high-density sEMG recordings. The discharge information of motoneurons at the population level (i.e., the output signals of spinal cord) can reflect the descending neural command from the brain to the muscles. The derived neural drive signal represents the neural command as binary motoneuron firing events, and can overcome the interference from MUAP variations or external interference during signal acquisition. Previous studies have shown that the derived neural drive signals can better predict muscle forces, compared with the global EMG features [19], [20]. However, previous research primarily focuses on force predictions at constant or slow varying levels of isometric muscle contractions. The neural-drive-based prediction of joint kinematics under dynamic movements has not been evaluated.

Accordingly, our study systematically investigated the prediction of joint angles of individual fingers using the neural-drive-based approach. The individual finger movements were first classified using the linear discriminant analysis (LDA) classifier on multi-channel EMG signals of the extensor digitorum communis muscles. The LDA method has been shown

Chenyun Dai is with the Department of Electrical Engineering at Fudan University (email: chenyundai@fudan.edu.cn)

Xiaogang Hu is with the Joint Department of Biomedical Engineering at University of North Carolina-Chapel Hill and NC State University (email: xiaogang@unc.edu

to be a robust and efficient approach for EMG-based pattern recognition [21]. Motoneuron discharge events were extracted through high-density EMG decomposition, and were then pooled into a composite train. The average discharge frequency of the composite discharge events was calculated to estimate the neural drive. The metacarpophalangeal (MCP) joint angle of individual fingers was predicted using a second-order polynomial regression of the derived neural drive signals. To evaluate the prediction performance, we compared the neural-drive-based approach with the global EMG-based approach. Our results showed that, compared with the global EMG-based method, the neural-drive-based approach can better predict the joint angles with a higher correlation (R^2) and a lower root-mean-square error (RMSE) between the predicted and the measured joint angles. Our findings indicate that the neural-drive-based approach has great promise in predicting joint kinematics of individual fingers during dynamic movements. A preliminary study involving two subjects with limited analyses has been reported previously [22].

II. Methods

A. Subjects

After providing the written informed consent, eight intact subjects (six males, two females; aged 26.6±5.6 years) participated in the experiment. The experimental protocol and all data analyses were approved by the Institutional Review Board of the University of North Carolina at Chapel Hill.

B. Experimental Protocol

Subjects were seated at a straight-back chair with the right shoulder comfortably abducted approximately 45°, their forearm fully pronated and supported on the soft foam pads, and the MCP joints of the four fingers (index, middle, ring, and little) naturally bent with approximately 120° to the palm (resting state). During the experiment, subjects extended one designated finger from the naturally relaxed position (~120° to the palm) to maximum joint angle they can extend, and then gradually decreased the extension angle back to the initial position. The subjects were asked to minimize muscle co-contractions. The movement speed was guided by a custom-built MATLAB (MathWorks Inc) display (see Fig. 1A). The red curve continuously moved over the blue trajectory as a series of positive phases of a sine wave at two different speeds (2 s or 5 s for each phase). Take the 2 s movement condition as an example, the subjects needed to reach maximum extension from resting in 1 s, and took 1 s to come back to the resting state. Subjects were asked to follow the movement of the red curve, with the full relaxation at the sine wave peak value of 1 and the resting state at the minimum value of 0. A 1-s resting was provided between two adjacent phases. The finger extension movements were repeated five times within each trial, and five trials were performed. Therefore, a total of twenty-five extension movements were acquired for each condition (per finger or movement speed). A 30-s rest period was provided between two consecutive trials to avoid cumulative fatigue. The order of designated finger or movement speed was randomized. Overall, a total of 40 trials (four fingers × two movement speeds × five trials) were recorded for each subject.

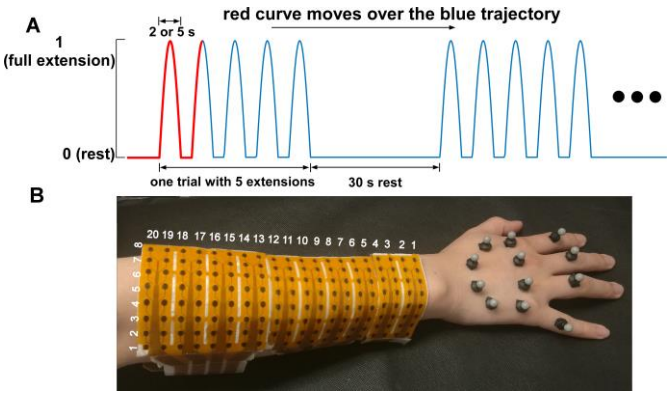

Fig. 1. Experimental setup. A: The visual display as a guide for finger movement speed. Each positive phase of the sine wave represents one extension movement. Each trial contains five extensions, and five trials were recorded in total. B: The 8 × 20 high-density electrode grid recorded the surface EMG signals from the extensor digitorum communis (EDC) muscle. The reflective markers measured the angles of the metacarpophalangeal joints.

C. Finger Motion Tracking and EMG Recording

The angles of the MCP joints of each finger were acquired using an 8-camera Optitrack system (Natural Point Inc, Corvallis, OR). We attached three 6-mm reflective markers to each finger (see Fig. 1B). The 3D positions of the markers were recorded using the motion capture software (Motive, NaturalPoint Inc, Corvallis, OR) with a sampling rate of 120 Hz.

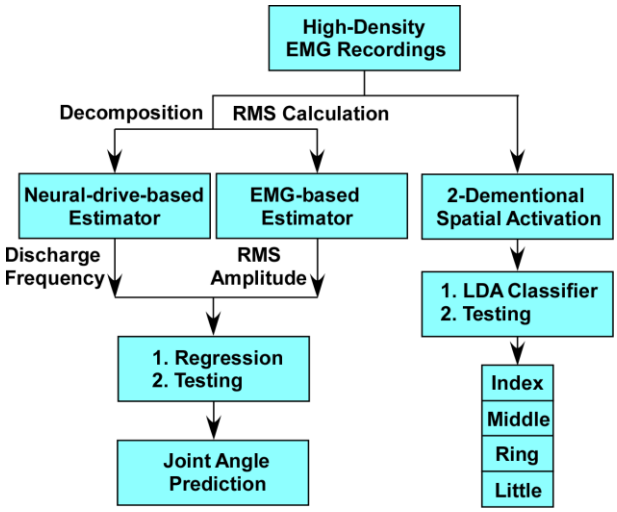

Fig. 2. Block diagram of the data analysis. RMS: root mean square value, LDA: linear discriminant analysis.

Only EMG signals of the extensor muscles were recorded, since finger flexion movement was completed by the inertia of the fingers with relaxed extensor muscle. The surface EMG signals were acquired with the flexible high-density electrode grids (ELSCH064NM3, OT Bioelettronica, Torino, Italy). A total of 160 recording electrodes (8 × 20, Fig. 1B), with an inter-electrode distance of 10 mm in both directions, were placed over the extensor digitorum communis (EDC) muscle. Prior to the electrode placement, gel was applied to each electrode sensor to improve conductivity. The skin above the

EDC muscle was also cleaned with abrasive gel and then scrubbed with alcohol pads to further reduce the impedance between the electrodes and the skin. The EMG-USB2+ system (OT Bioelettronica, Torino, Italy) amplified and filtered the EMG signals (with a gain of 1000 and a band-pass filter of 10-900 Hz), and sampled at 2048 Hz with a 12-bit resolution.

D. Data Analysis

All the data were analyzed offline using MATLAB. The block diagram of the data analysis procedures is illustrated in Fig. 2. We began by identifying individual finger movement. Previous studies [23], [24] have shown that the individual finger extension movement is driven by the distinct compartments of the EDC muscles. Therefore, the muscle activation regions were localized and distinguishable during individual finger movements, covering one third or less of the entire muscle [24]. Accordingly, the 2D root-mean-square values of the 8 × 20 monopolar EMG grid were calculated as the spatial features, and the LDA classifier was used to identify each finger extension. For each condition (finger or movement speed), ten out of the twenty-five extension movements were randomly selected to train the parameters of the classifier, and the remaining fifteen trials were used to test the performance of the classifier within each subject. A total of four classes (index, middle, ring, or little) were evaluated, and only testing results were reported. The movement speed was evaluated separately.

Given that localized activation regions of the EDC muscle were associated with individual finger movements, a large number of EMG channels contained mostly baseline noise during individual finger movements (Fig. 3). To reduce the influence of noise on joint angle prediction, only 8 × 8 channels with higher signal amplitude were used for the estimation [20]. Specifically, the channels from column 1-8, 13-20, and 7-14 (Fig. 1B) were used for the index, middle, and ring/little finger joint estimations, respectively. Since the muscle activation regions of the ring and little fingers mostly overlapped, the same columns were used for these two fingers.

The EMG signals in the selected 64 channels were then decomposed into individual MU spike trains using the fast independent component analysis (FastICA) method [25]. To obtain enough information for the acquisition of the MU spike trains, the decomposition was performed for each trial with 5 extension movements. The accuracy of the algorithm has been verified by previous studies [26]–[28]. The detailed steps and the parameter selection of the algorithm were described in [28]. Briefly, the decomposition includes four main steps: 1) extend the raw EMG signals by adding the delayed replicas of each original channel [29]; 2) whiten the extended signals using eigenvalue decomposition; 3) deconvolute the whitened EMG signals using the FastICA algorithm; and 4) detect the discharge timings using *k-means* clustering [30].

Two post-processing steps were performed to increase the reliability of the decomposition. First, the silhouette measure (SIL) was used to remove the MU spike trains with low clustering separation [28]. The SIL is a clustering index that measures how distinguishable the extracted MU was, compared with the activities of all remaining MUs and background noise during the *k-means* clustering. Any MU spike trains with SIL<0.8 were removed [31]. Second, the algorithm may converge to the same MU multiple times as well as its delayed replicas. Therefore, if a pair of MU spike trains had >50% synchronized firings within ± 1ms after adjusting the time delay, only the MU spike train with a higher SIL was reserved. The 50% synchronization was selected as the threshold because the MU discharge synchronization level could reach up to 20 or 30 % for a pair of MUs [32]. The use of 50% synchronization can avoid filtering two different MUs with strong firing synchronization. After the preprocessing procedures, all the retained MU spike trains were pooled into one composite spike train. The mean discharge frequency of the composite spike train was used to estimate the neural drive.

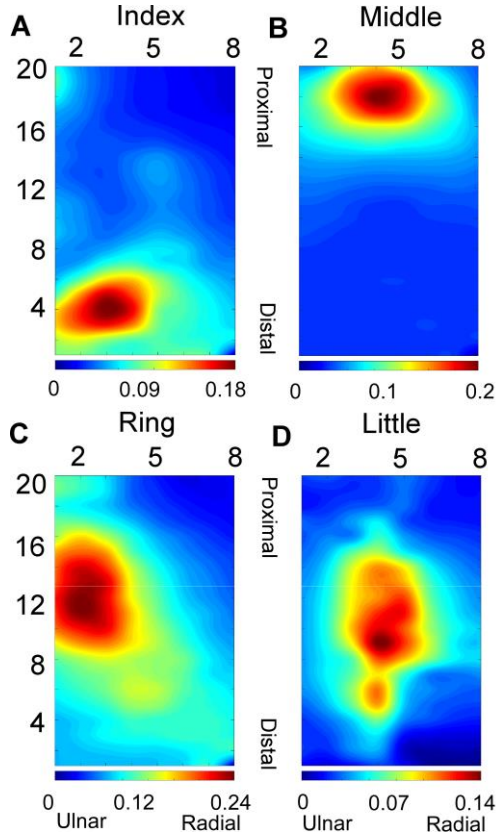

Fig. 3. Two-dimensional heat map (root mean square value) during individual finger movements. A: Index. B: Middle. C: Ring. D: Little. X- or Y-axis labels represent the column or row numbers of the electrode grid.

In addition, the conventional EMG-amplitude-based approach was used as a control condition for joint angle estimation. Specifically, the same selected 8 × 8 EMG signals used for decomposition were band-pass filtered (4th order Butterworth with a cut-off frequency at 50 and 500 Hz) to reject motion artifacts and high frequency background noise. Then, the signals were notch filtered (2nd order notch filter at 60 Hz with a bandwidth of 1 Hz) to eliminate the power line noise. Lastly, the root-mean-square value of the processed 8 × 8 EMG signals were calculated, and then averaged across all 64 channels. The mean root-mean-square value was used as an estimate of the EMG amplitude.

A 200 ms sliding window with a moving step of 50 ms was

applied to smooth both the EMG amplitude and the neural drive estimation. A larger size of the moving window can produce a smoother prediction, but can lead to a longer time delay. To meet the constraints of real-time control, a 200 ms window with an update rate of 50 ms is considered acceptable [18]. The EMG amplitude and the neural drive estimation were then associated with the joint angle using a regression analysis. Specifically, during the regression analysis, two of the five trials (each trial contained five extension movements) were randomly selected to calculate the regression coefficients using the EMG amplitude or neural drive and the measured joint angles. The remaining trials were used as the testing trials to predict the joint angles. All possible combinations of extension movements were used for regression/training. We also performed cross-validation using all possible combinations of extension movements (not in training) for testing. In addition, three regression models, linear, quadratic, and second-order polynomial, were tested with the Bayesian information criterion (BIC) [33] to acquire the parsimonious (simplest and best) model. The performance of the joint angle prediction was evaluated by the R^2 and RMSE values between the estimated values and the actual joint movement. Both the regression and testing results were reported in the Results section.

E. Statistical Analysis

All statistical analyses were performed in SPSS 24 (IBM). The performance of the joint angle prediction was investigated on three factors [*movement speed* × *finger* × *estimation method*] using a repeated measures analysis of variance (ANOVA). Prior to the ANOVA, the R^2 values were transformed using an *arcsine-square-root* transformation ($Y = arcsin\sqrt{P}$, where P is the R^2, and Y is the result of the transformation), given that the data are bounded between 0 and 1, and the transformation can release the bound. Normality of the residuals was tested for each of the ANOVA in the Results section, using the Shapiro-Wilk test. In addition, the histograms, Q-Q plots and box plots of the residuals were manually inspected for each condition. The homogeneity test was performed to verify the equal variance assumption using Levene's test. Tests considered all the three factors: *finger*, *movement speed,* and *estimation method*. The tests affirmed normality ($p > 0.05$ in the Shapiro-Wilk test) with equal variances ($p > 0.05$ in the Levene's test). The finger classification results were also tested using one-way ANOVA. *Post hoc* pairwise comparisons with Bonferroni corrections were conducted when necessary. The significant level of $p < 0.05$ was used.

III. Results

A. Finger Classification

We first investigated the classification accuracy of specific finger movement using high-density EMG signals. Fig. 4 shows the overall classification results and the corresponding confusion matrix. The overall accuracy of the classification results was 98.6±1.37%, and the accuracy was 99.6%, 99.8%, 98.3%, and 96.7% for the index, middle, ring, and little fingers, respectively. The one-way ANOVA on the *finger* factor found a significant difference [$F(3,21) = 11.013$, $p = 0.007$]. Further *post hoc* analysis showed that the classification accuracy of the index and middle fingers was higher than the other two fingers, and the little finger has the highest possibility to be detected as a different finger. Although the ANOVA results showed significant difference between fingers, numerically, the difference was within 3.1% between fingers.

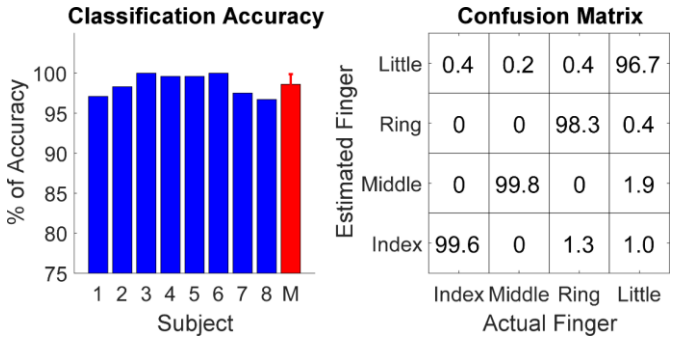

Fig. 4. The overall results of finger classification. Left: the classification accuracy of each subject. 'M' represents the mean accuracy of all the subjects. Right: confusion matrix. For example, if '0.4' is shown in the index column and little row, it means the classifier falsely detected the index finger as the little finger 0.4% out of the entire index finger identification.

B. EMG Decomposition

TABLE I
Overall Results of EMG Decomposition

Finger	Numbers of Motor Units		Mean Minimal Firing Rate /Hz		Mean Maximal Firing Rate /Hz	
	Fast	Slow	Fast	Slow	Fast	Slow
Index	14±4	11±5	6.3±1.7	5.7±2.2	18.6±3.6	15.9±1.5
Middle	16±7	12±4	6.7±1.4	6.6±3.1	21.1±4.3	19.1±2.9
Ring	15±5	12±4	6.6±2.9	6.7±2.2	18.2±3.9	17.7±2.2
Little	15±6	13±7	6.5±1.9	6.4±1.2	17.6±3.5	16.7±1.8

We then decomposed the high-density EMG recordings into individual MU spike trains. The overall decomposition results are summarized in Table 1. The numbers of decomposed MUs, after filtering, ranged from 14 to 16 for fast movements and 11 to 13 for slow movements. The mean firing rate of decomposed MU spike train ranged from 5.7 Hz to 21.1 Hz. The mean minimal firing rate represented the minimal firing rate of the decomposed MUs and then averaged across subjects. The mean maximal firing rate represented the maximal firing rate of the decomposed MUs and then averaged across subjects. Three three-way ANOVAs combined with *Post hoc* pairwise comparisons were performed on the number of MUs, mean minimal firing rate and mean maximum firing rate. The main findings of statistical tests showed that (1) the fast movement can detect a greater number of MUs than the slow movement ($p < 0.05$); (2) the mean maximal firing rate of middle finger was higher than the rest of the fingers ($p < 0.05$); and (3) the mean maximal firing rate of fast movements of index and middle fingers was higher than that of slow movement ($p < 0.05$).

C. Joint Angle Prediction

The MU spike trains were then pooled into a composite spike train. The mean frequency of the composite spike train was calculated with a 200 ms smoothing window to predict the joint angle movement. In addition, the root-mean-square values of

EMG signals with the same window parameters were also calculated to predict the joint angles. Three regression models: linear, quadratic, and second-order polynomial were used to identify the parsimonious function. The quadratic and second-order polynomial functions were used to account for curvilinear relation between the joint angle and the neural drive (or EMG amplitude), due to changes in muscle force moment arm during movements. The BIC measurement showed that the second-order polynomial model had the lowest BIC values for both neural-drive-based and EMG-amplitude-based regression analysis. Therefore, the second-order polynomial function was used for further analysis, and the results of the linear and quadratic functions were not reported. Given the collinearity between the linear term and the squared term, only the overall fit was evaluated, and the individual regression coefficient was not interpreted. The histogram illustrating the distribution of the residuals for the polynomial regression was also visually inspected to ensure that the residuals were normally distributed. Fig. 5 shows the sample time-series of joint angle predictions of both the EMG-amplitude-based and the neural-drive-based approaches. The neural-drive-based approach exhibited a higher R^2 and a lower RMSE value than the EMG-amplitude-based estimation. A more stable estimation during the continuous extension, especially at the full extension angle, was observed using the neural-drive-based approach.

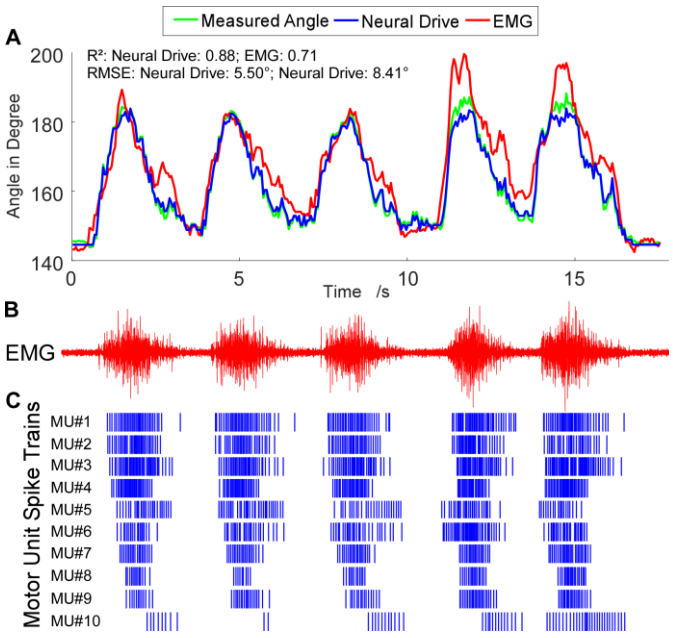

Fig. 5. A: Example time-series plots of joint angle prediction using both EMG-amplitude-based and neural-drive-based approaches. B: One representative EMG channel with the largest root mean square (RMS) value. C: Motor unit (MU) spike trains. Blue bars represent discharge timings of individual MUs. The MUs are presented in recruitment order. Namely, MU #1 was recruited first, and MU #10 was recruited last.

The overall performance of the two methods for each finger and movement speed are summarized in Fig. 6. For the R^2 of the regression, the values varied from 0.69 to 0.86 for the neural-drive-based estimates, and varied from 0.66 to 0.81 for the EMG-amplitude estimates. A three-way repeated measures ANOVA was performed on the three factors—movement *speed*, *finger,* and *method* (p = 0.8 in the Levene's test). The results showed a significant difference on the factors of *speed* [F(1,7) = 7.093, p = 0.032] and *method* [F(1,7) = 9.611, p = 0.017], but found no significant difference on the factor of *finger* [F(3,21) = 1.057, p = 0.389]. A further post hoc analysis found that the neural-drive-based estimates were always better than the EMG-amplitude-based estimates at both fast (p = 0.006) and slow (p = 0.043) movement speeds, and the fast movement showed a better estimate than the slow movement only for the neural-drive-based estimates (p = 0.005). For the RMSE between the estimated and the measured joint angles, the absolute RMSE values were normalized by the maximum angle of individual fingers. The three-way repeated measure ANOVA was performed on the normalized RMSE values. The ANOVA (p = 0.1 in the Levene's test) showed that a significant interaction between the factors of *speed* and *method* [F(1,7) = 6.039, p = 0.044], but found no significant difference on the factor of *finger* [F(3,21) = 0.540, p = 0.660]. Further post hoc analysis showed that the neural-drive-based estimates always had lower RMSE than the EMG-amplitude-based estimates on both fast (p = 0.008) and slow (p = 0.044) movement speeds, and the fast movement showed a lower RMSE than the slow movement only for the neural-drive-based estimates (p = 0.006).

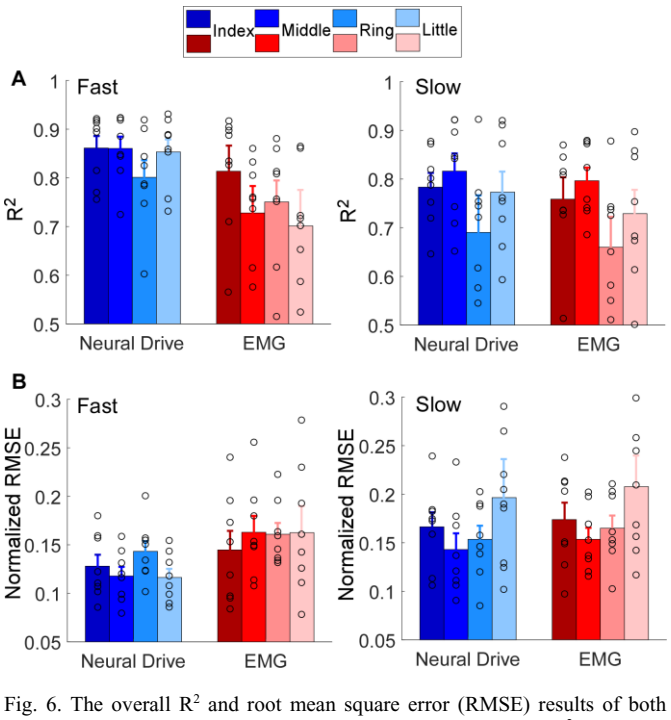

Fig. 6. The overall R^2 and root mean square error (RMSE) results of both neural-drive-based and EMG-amplitude-based approaches. A: R^2 values. B: normalized RMSE values. The error bars represent the standard errors across eight subjects. Individual circles represent individual subjects.

Finally, the overall difference of R^2 and RMSE values during regression and testing are summarized in Fig. 7. The grand mean value of each condition was calculated. A small difference (~0.03 for R^2 values and ~0.02 for RMSE values) was found between the regression and testing results for both approaches. The results indicated that both approaches exhibited a consistent estimate across different trials.

IV. Discussion

In this study, we estimated the joint kinematics of individual fingers based on populational MU firing frequency, which reflected the descending neural drive to the motoneuron pool. The MU firing properties were obtained from high-density EMG recordings of finger extensor muscles. The dynamic movement of each finger was first classified based on spatial patterns of muscle activations during individual finger movements. The joint angles were estimated using a second-order polynomial regression. The performance of the joint angle prediction based on the derived neural drive was also compared with the global EMG-amplitude-based prediction. Our results showed that individual finger movement can be classified with high accuracy, and that the joint angle can be predicted accurately using the neural-drive-based approach. In addition, we showed that the neural-drive-based approach outperformed the EMG-amplitude-based approach. These findings indicate that the neural-drive-based approach had great promise in accurately predicting joint angles of individual fingers, which can potentially be used as a reliable human-machine interface signal.

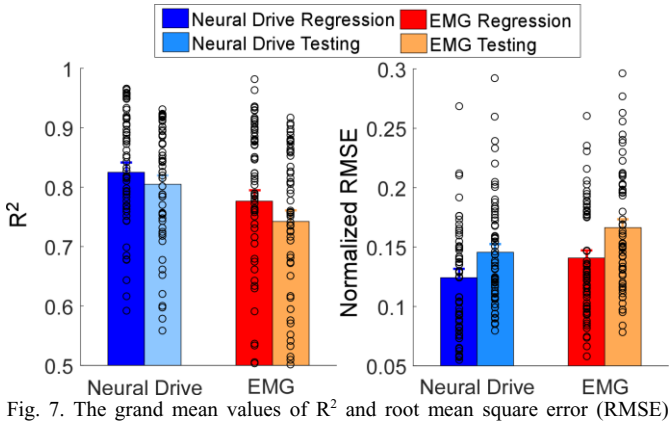

Fig. 7. The grand mean values of R^2 and root mean square error (RMSE) values between regression and testing results for both neural-drive-based and EMG-amplitude-based approaches. Individual circles represent individual regression or testing results.

A. Finger Classification

Individual finger extension is driven by the EDC muscle compartments in the forearm. The current study identified individual finger extension based on spatial patterns of activation from the EDC muscle. The synchronized finger extension can arise from mechanical couplings and neural control from common synaptic inputs among different fingers. The enslaving effect can bias the EMG amplitude estimation [35], [36]. Furthermore, because of the complex anatomical organization of the EDC, traditional EMG recordings may not accurately capture the muscle activations due to potential cross-talk [35]. On the other hand, EDC is a multi-compartment muscle [37], and distinct subpopulations of the motoneuron pool control the individual compartments of the EDC [38]. A previous study [24] has shown that the active compartments during individual finger extension are localized and spatially distinguishable. Therefore, the use of high-density EMG recordings, which can capture the activation patterns of the entire muscle, is an effective approach to extract the different spatial activation patterns during different finger movements. Our results showed that the average classification accuracy was > 98%. We also notice that the classification accuracy of the index, middle, and ring fingers are slightly higher than that of the little finger. The low accuracy can arise from the fact that the activation of the little finger spans a major surface region of the EDC muscle, and the index (distal), middle (proximal), and ring (central) fingers are relatively localized as shown in Fig. 3 and a previous study [24].

B. EMG Decomposition

Our results showed that the FastICA-based algorithm can extract MU behaviors under dynamic movements. The dynamic contraction conditions impose challenges to the algorithm, largely due to muscle fiber shift beneath the recording electrodes, which can lead to variations of the EMG signals. Specifically, the shift of the muscle fibers can affect the MUAP waveforms (in both shape and amplitude) recorded at a particular channel. Furthermore, external factors, including motion artifacts and changes in electrode-electrolyte contact during dynamic movements, can further aggravate the accuracy of the decomposition. It has been reported that only about 50% of common MUs can be found between two different trials for a given task, due to changes of MUAP waveform [31]. However, our results showed that the FastICA-based algorithm was not sensitive to the variation of MUAP under the controlled dynamic movement condition, providing high decomposition yield with > 10 MUs per task. The decomposition yield was similar to the results reported in a recent study under dynamic wrist movement conditions [31].

During the experiment, different speeds of extension movements were evaluated. Our results showed that the decomposed MU discharge events can still predict the fast changes of recruitment and derecruitment during the relatively fast dynamic motions. In addition, we noticed that the fast movement can yield more MUs than the slow movement. It is likely that the fast movement required higher levels of muscle contractions, and, consequently, more MUs were recruited [39]. A larger number of MU spike trains can better represent the population behavior of the motoneuron pool, which can lead to a better prediction of the neural drive.

C. Joint Angle Prediction

The results showed a consistently better performance of neural-drive-based approach for joint angle predictions, compared with the classic EMG-amplitude-based approach. The neural drive was derived from the populational discharge frequency of the composite spike train, which has several advantages over the EMG-amplitude-based approach. First, the binary spike train was minimally influenced by the MUAP variation, such as the change or cancellation of the waveforms. Second, the neural-drive-based approach was not sensitive to background noise, including variations in the baseline noise and motion artifacts. These factors tend to bias the joint angle estimations using the EMG-amplitude-based approach,

especially during dynamic contractions.

We also noticed that the fast movements showed a better performance than the slow movements using the neural-drive-based approach. As we have discussed earlier, more MUs can be recruited from fast movements [39], leading to better estimates of the joint movements. The speed of 5 s per extension was relatively slow, likely to be much slower than a majority of daily activities, only requiring a small amount of muscle activations. Nevertheless, we still found that the neural-drive-based approach was slightly better than the EMG-amplitude-based approach under the slow movement condition. The 2-s movement speed condition is likely to be more representative to daily activities, and we found more distinct differences in the angle prediction performance between the two approaches.

To further evaluate the neural-drive-based approach, model regression and testing analysis was performed on individual fingers across different trials. We found a minor difference on the goodness of fit (R^2) and angle prediction errors (RMSE values) between the regression and testing, and similar performance was observed across individual fingers. These outcomes indicated the stability of using the neural-drive-based approach across different fingers, consistent with earlier studies [40]. In addition, we used the BIC index to select the simplest and best model for the joint angle predictions. A complex model can capture more variations in the existing data, but can over-fit the data and lose generalizability to new observations. In our study, the second-order polynomial model was selected. The model selection was consistent with earlier observations, which showed non-linearity between the joint movements and the EMG signals [41].

D. Limitations

In our current study, all the analyses were performed offline. The EMG-amplitude-based approach is suitable for real-time processing, because minimal computation is required. However, the computational load of the neural-drive-based approach is high, largely during the EMG decomposition process. FastICA indeed is more efficient compared with other ICA algorithms, but online calculation is still a challenge. As a result, real-time joint angle estimation was not tested using MU firing activities in the current study. Nonetheless, online decomposition can be achieved as shown in previous studies [42], [43]. The strategy of online decomposition is to acquire the separation matrix for the extraction of motoneuron discharge events using a short initial data segment (approximately 5-10 s, which typically requires approximately 10 s for computation). The subsequent MU discharge information can be obtained iteratively by multiplying the separation matrix with the incoming data segments. The separation matrix may require periodic update during long-term use. In addition, it has also been shown that the performance of the real-time processing is worse than the offline processing [43], but the neural-drive-based approach is still beneficial compared with the EMG-amplitude-based approach during prolonged muscle activation. Although the performance difference in joint angle estimation was small between the neural-drive-based and the EMG-amplitude-based approach in the short trial period. We are optimistic that the neural-drive-based approach will show more stable performance over time, which is critical for human-machine interactions.

V. Conclusion

The current study shows that individual finger movements can be identified, and the individual finger joint angles can be continuously predicted using populational MU firing events. The classification accuracy of individual finger movements was > 96% using the spatial patterns of muscle activations. The neural-drive-based approach, through high-density EMG decomposition, provided a more accurate estimation of the finger movements, compared with the classic EMG-amplitude-based approach. Overall, the neural-drive-based approach can further facilitate the development of human-machine interactions. This technique can shift the interface signal from the macro EMG to populational MU activities, which is more robust to external interference. Our results verified the feasibility of using the neural-drive-based approach to reliably and continuously estimate the joint angles of individual fingers. These findings provide support on an alternative interface signal that could be used for human-machine interactions.

References

[1] S. Hesse, H. Schmidt, C. Werner, and A. Bardeleben, "Upper and lower extremity robotic devices for rehabilitation and for studying motor control," *Curr. Opin. Neurol.*, vol. 16, no. 6, pp. 705–710, 2003.

[2] H. S. Lo and S. Q. Xie, "Exoskeleton robots for upper-limb rehabilitation: State of the art and future prospects," *Med. Eng. Phys.*, vol. 34, no. 3, pp. 261–268, 2012.

[3] G. Kwakkel, B. J. Kollen, and H. I. Krebs, "Effects of robot-assisted therapy on upper limb recovery after stroke: a systematic review," *Neurorehabil. Neural Repair*, vol. 22, no. 2, pp. 111–121, 2008.

[4] T. A. Kuiken *et al.*, "Targeted muscle reinnervation for real-time myoelectric control of multifunction artificial arms," *Jama*, vol. 301, no. 6, pp. 619–628, 2009.

[5] D. W. Tan, M. A. Schiefer, M. W. Keith, J. R. Anderson, J. Tyler, and D. J. Tyler, "A neural interface provides long-term stable natural touch perception," *Sci. Transl. Med.*, vol. 6, no. 257, pp. 257ra138--257ra138, 2014.

[6] M. A. Lebedev and M. A. L. Nicolelis, "Brain--machine interfaces: past, present and future," *TRENDS Neurosci.*, vol. 29, no. 9, pp. 536–546, 2006.

[7] X. Navarro, T. B. Krueger, N. Lago, S. Micera, T. Stieglitz, and P. Dario, "A critical review of interfaces with the peripheral nervous system for the control of neuroprostheses and hybrid bionic systems," *J. Peripher. Nerv. Syst.*, vol. 10, no. 3, pp. 229–258, 2005.

[8] T. Boretius *et al.*, "A transverse intrafascicular multichannel electrode (TIME) to interface with the peripheral nerve," *Biosens. Bioelectron.*, vol. 26, no. 1, pp. 62–69, 2010.

[9] J. L. Collinger *et al.*, "High-performance neuroprosthetic control by an individual with tetraplegia," *Lancet*, vol. 381, no. 9866, pp. 557–564, 2013.

[10] L. H. Smith, T. A. Kuiken, and L. J. Hargrove, "Real-time simultaneous and proportional myoelectric control using intramuscular EMG," *J. Neural Eng.*, vol. 11, no. 6, p. 66013, 2014.

[11] F. Tenore, A. Ramos, A. Fahmy, S. Acharya, R. Etienne-Cummings, and N. V Thakor, "Towards the control of individual fingers of a prosthetic hand using surface EMG signals," in *Engineering in Medicine and Biology Society, 2007. EMBS 2007. 29th Annual International Conference of the IEEE*, 2007, pp. 6145–6148.

[12] C. Castellini and P. van der Smagt, "Surface EMG in advanced hand prosthetics," *Biol. Cybern.*, vol. 100, no. 1, pp. 35–47, 2009.

[13] E. A. Clancy, C. Martinez-Luna, M. Wartenberg, C. Dai, and T. R. Farrell, "Two degrees of freedom quasi-static EMG-force at the wrist using a minimum number of electrodes," *J. Electromyogr. Kinesiol.*, vol. 34, 2017.

[14] C. Dai, B. Bardizbanian, and E. A. Clancy, "Comparison of Constant-Posture Force-Varying EMG-Force Dynamic Models about the Elbow," *IEEE Trans. Neural Syst. Rehabil. Eng.*, vol. 25, no. 9, 2017.

[15] C. Dai and X. Hu, "Extracting and Classifying Spatial Muscle Activation Patterns in Forearm Flexor Muscles Using High-Density Electromyogram Recordings," *Int. J. Neural Syst. vol. 29, no. 1850025, 2019*

[16] K. G. Keenan, D. Farina, K. S. Maluf, R. Merletti, and R. M. Enoka, "Influence of amplitude cancellation on the simulated surface electromyogram," *J. Appl. Physiol.*, vol. 98, no. 1, pp. 120–131, 2005.

[17] Y. Zheng, and X. Hu, "Interference removal from electromyography based on independent component analysis," *IEEE Trans. Neural Syst. Rehabil. Eng.*, vol 27 no. 5, pp.887-894. 2019.

[18] D. Farina *et al.*, "Man/machine interface based on the discharge timings of spinal motor neurons after targeted muscle reinnervation," *Nat. Biomed. Eng.*, vol. 1, p. 25, 2017.

[19] C. K. Thompson *et al.*, "Robust and accurate decoding of motoneuron behaviour and prediction of the resulting force output," *J. Physiol.*, 2018.

[20] C. Dai, Y. Zheng, and X. Hu, "Estimation of Muscle Force Based on Neural Drive in a Hemispheric Stroke Survivor," *Front. Neurol.*, vol. 9, p. 187, 2018.

[21] A. Phinyomark, F. Quaine, S. Charbonnier, C. Serviere, F. Tarpin-Bernard, and Y. Laurillau, "EMG feature evaluation for improving myoelectric pattern recognition robustness," *Expert Syst. Appl.*, vol. 40, no. 12, pp. 4832–4840, 2013.

[22] C. Dai, Y. Cao, and X. Hu, "Estimation of Finger Joint Angle Based on Neural Drive Extracted from High-Density Electromyography," in *2018 40th Annual International Conference of the IEEE Engineering in Medicine and Biology Society (EMBC)*, 2018, pp. 4820–4823.

[23] D. A Keen and A. J. Fuglevand, "Common input to motor neurons innervating the same and different compartments of the human extensor digitorum muscle.," *J. Neurophysiol.*, vol. 91, no. 1, pp. 57–62, 2004.

[24] X. Hu, N. L. Suresh, C. Xue, and W. Z. Rymer, "Extracting extensor digitorum communis activation patterns using high-density surface electromyography," *Front. Physiol.*, vol. 6, no. OCT, pp. 1–9, 2015.

[25] A. Hyvärinen and E. Oja, "Independent component analysis: algorithms and applications," *Neural networks*, vol. 13, no. 4, pp. 411–430, 2000.

[26] F. Negro, S. Muceli, A. M. Castronovo, A. Holobar, and D. Farina, "Multi-channel intramuscular and surface EMG decomposition by convolutive blind source separation," *J. Neural Eng.*, vol. 13, no. 2, p. 26027, 2016.

[27] C. Dai and X. Hu, "Independent component analysis based algorithms for high-density electromyogram decomposition: Experimental evaluation of upper extremity muscles," *Comput. Biol. Med.*, vol. 108, pp. 42–48, 2019.

[28] C. Dai and X. Hu, "Independent component analysis based algorithms for high-density electromyogram decomposition: Systematic evaluation through simulation," *Comput. Biol. Med.*, vol. 109, pp. 171-181, 2019.

[29] A. Holobar and D. Zazula, "Multichannel blind source separation using convolution kernel compensation," *IEEE Trans. Signal Process.*, vol. 55, no. 9, pp. 4487–4496, 2007.

[30] Y. Ning, X. Zhu, S. Zhu, and Y. Zhang, "Surface EMG decomposition based on K-means clustering and convolution kernel compensation," *IEEE J. Biomed. Heal. informatics*, vol. 19, no. 2, pp. 471–477, 2015.

[31] T. Kapelner, F. Negro, O. C. Aszmann, and D. Farina, "Decoding Motor Unit Activity From Forearm Muscles: Perspectives for Myoelectric Control," *IEEE Trans. Neural Syst. Rehabil. Eng.*, vol. 26, no. 1, pp. 244–251, 2018.

[32] W. Yao, R. J. Fuglevand, and R. M. Enoka, "Motor-unit synchronization increases EMG amplitude and decreases force steadiness of simulated contractions," *J. Neurophysiol.*, vol. 83, no. 1, pp. 441–452, 2000.

[33] G. Schwarz and others, "Estimating the dimension of a model," *Ann. Stat.*, vol. 6, no. 2, pp. 461–464, 1978.

[34] N. M. Razali, Y. B. Wah, and others, "Power comparisons of shapiro-wilk, kolmogorov-smirnov, lilliefors and anderson-darling tests," *J. Stat. Model. Anal.*, vol. 2, no. 1, pp. 21–33, 2011.

[35] M. Solomonow *et al.*, "Surface and wire EMG crosstalk in neighbouring muscles," *J. Electromyogr. Kinesiol.*, vol. 4, no. 3, pp. 131–142, 1994.

[36] N. van Beek, D. F. Stegeman, J. C. Van Den Noort, D. H. E. J. Veeger, and H. Maas, "Activity patterns of extrinsic finger flexors and extensors during movements of instructed and non-instructed fingers," *J. Electromyogr. Kinesiol.*, vol. 38, pp. 187–196, 2018.

[37] V. M. Zatsiorsky, Z. M. Li, and M. L. Latash, "Coordinated force production in multi-finger tasks: finger interaction and neural network modeling.," *Biol. Cybern.*, vol. 79, pp. 139–150, 1998.

[38] C. Dai, H. Shin, B. Davis, and X. Hu, "Origins of Common Neural Inputs to Different Compartments of the Extensor Digitorum Communis Muscle," *Sci. Rep.*, vol. 7, no. 1, 2017.

[49] J. Wessberg and N. Kakuda, "Single motor unit activity in relation to pulsatile motor output in human finger movements," *J. Physiol.*, vol. 517, no. 1, pp. 273–285, 1999.

[40] C. Dai, Y. Cao, and X. Hu, "Prediction of Individual Finger Forces Based on Decoded Motoneuron Activities," *Ann. Biomed. Eng.*, vol. 47, no. 6, pp. 1357-1368, 2019.

[41] R. B. Stein and R. E. Kearney, "Nonlinear behavior of muscle reflexes at the human ankle joint," *J. Neurophysiol.*, vol. 73, no. 1, pp. 65–72, 1995.

[42] V. Glaser, A. Holobar, and D. Zazula, "Real-time motor unit identification from high-density surface EMG," *IEEE Trans. neural Syst. Rehabil. Eng.*, vol. 21, no. 6, pp. 949–958, 2013.

[43] Y. Zheng, and X. Hu, "Real-time isometric finger extension force estimation based on motor unit discharge information," *J. Neural Eng.*, 2019.